RSC Advances

PAPER

View Article Online
View Journal | View Issue

Cite this: *RSC Adv.*, 2024, **14**, 36622

Silicotungstate@ZIF-67 as an effective catalyst for an extraction and oxidative desulfurization system

Lijun Xu, Qian Tong and Bing Hu*

Received 18th September 2024
Accepted 23rd October 2024

DOI: 10.1039/d4ra06736c

rsc.li/rsc-advances

Through a simple room-temperature process, different amounts of Keggin-type quaternary ammonium silicotungstate were successfully encapsulated into the metal–organic framework (MOF) material ZIF-67. The catalysts were characterized using Fourier transform infrared (FT-IR) spectroscopy, X-ray powder diffraction (XRD), scanning electron microscopy (SEM), and BET analysis. An extraction and catalytic oxidation desulfurization system was studied using H_2O_2 as an oxidant and a deep eutectic solvent (DES) as an extractant. Using the 43.06%-SiW_{12}@ZIF-67 composite under optimal reaction conditions, DBT present in a model oil could be deeply and effectively removed. The catalyst was reused 6 times, and the desulfurization rate still exceeded 90%. Finally, a possible desulfurization mechanism is proposed.

1. Introduction

As society develops, the living standards of people continue to improve, driving the rapid growth of the transportation industry. Despite the global efforts to develop new energy sources to replace fossil fuels, they still account for around 85% of global energy production.[1,2] As a result, gasoline and diesel will remain the main sources of power for the foreseeable future. Sulfur-containing compounds in crude oil are one of the major impurities, and sulfur oxides (SO_x) produced during combustion lead to environmental problems such as acid rain and haze, posing a serious hazard to human health and ecological safety.[3–5] Therefore, countries worldwide have introduced laws and regulations to strictly control the sulfur content in gasoline and diesel fuel to reduce pollution.[6] China has fully implemented the national VI standard, with sulfur content not exceeding 10 ppm.[7] Consequently, desulfurization of fuels remains a significant research area, aiming to develop effective technologies for predominantly dealing with high molecular weight aromatic sulfur compounds from fuels.

The most technologically mature and widely used process is traditional hydrodesulfurization (HDS).[8,9] HDS can effectively remove aliphatic and acyclic sulfides, but it is less effective in removing thiophene compounds, which have complex structures, high boiling points, and high spatial site resistance.[10–12] Consequently, as a relatively immature non-hydrodesulfurization technology (biological desulfurization, adsorption desulfurization, extraction desulfurization, and oxidative desulfurization), it has been the subject of extensive research interest owing to its potential for the removal of various sulfides, especially thiophene and its derivatives, at lower temperatures and with reduced energy consumption.[13–17] Among the various methods mentioned, oxidative desulfurization has emerged as a prominent approach for the removal of organic sulfur compounds through oxidation under mild experimental conditions.[18,19] However, a single oxidative desulfurization (ODS) technology is often insufficient for achieving deep desulfurization of fuels. In recent years, oxidative desulfurization has frequently been coupled with extractive desulfurization or assisted by catalysts to achieve the deep removal of aromatic sulfides.[20]

Deep eutectic solvents (DESs), which have properties similar to ionic liquids (ILs) and are therefore also known as ionic liquid analogs, have the advantages of non-toxicity, cost-effectiveness, excellent degradability, and simple preparation processes and are a new type of green and replaceable solvents.[21–24] Atoms capable of forming hydrogen bonds in DESs can be combined with sulfides with lone pairs of electrons as Lewis bases. Li *et al.* first applied DESs in the field of extraction desulfurization.[25] The high stability of DESs in water and oxygen, coupled with their excellent solubility in water, makes them an ideal candidate for introducing an oxidant to form an extraction-coupled oxidative desulfurization system.[26] This process is more effective than the traditional process to remove sulfides.

Polyoxometalates (POMs) are polymetallic oxygen cluster compounds composed of transition metals (V, Mo, W, *etc.*), oxygen, *etc.*, which have the advantages of structural stability and strong redox properties. Particularly, the most representative Keggin-type polyoxometalates, which have an $XM_{12}O_{40}^{m-}$ polyanion structure consisting of an oxygen-sharing MO_6 octahedron ($M = M_O^{VI}$, W^{VI}, V^V, *etc.*) wrapped around a central tetrahedron, XO_4^{n-} ($X = P^V$, Si^{IV}, *etc.*) have demonstrated remarkable activity in the catalysis of sulfides.[27,28] It was found that the high activity of POM is due to the production of reactive

School of Materials and Chemical Engineering, Hubei University of Technology, Wuhan 430068, People's Republic of China. E-mail: hubing@hbut.edu.cn

species with peroxide bonds in the presence of an oxidant.[29–31] Zhu Y. *et al.* proposed that in the presence of excess H_2O_2, the complex $M(O)_n$ was peroxidized as well as decomposed to form the anionic peroxometallic complex $M(O_2)_n$, which provided a catalytically active center for sulfide removal.[32] Li J. *et al.* prepared a polyoxometalate $[C_2(MIM)_2]PW_{12}O_{40}$ as a catalyst, and proposed that the intermediate product $[PO_4\{W(O)(O_2)_2\}_4]^{3-}$ obtained by the oxidation of $[PW_{12}O_{40}]^{3-}$ plays a key role in the removal of DBT from model oil.[33] However, the synthesis cost of POM is high, and the amount of POM used in the catalytic oxidative desulfurization process is large. Usually, extractants are added or carriers are introduced to improve the desulfurization efficiency.

Metal–organic frameworks can be used as excellent materials to encapsulate POM due to their high specific surface area, ordered channels, good stability, structural diversity, and simple and adjustable characteristics.[34–36] Among them, the zeolite imidazole framework (ZIF) has the advantages of both being a molecular sieve and traditional MOF, and its appropriate cavities and windows ensure the effective encapsulation of POM.[37–40]

In this study, a series of composite materials (x%-SiW_{12}@-ZIF-67) were prepared by encapsulating different contents of quaternary ammonium silicotungstate $(TBA)_4SiW_{12}O_{40}$ into MOF material ZIF-67 and characterized by various methods. Then, they were used as catalysts in the extraction and oxidative desulfurization system to remove sulfides (BT, DBT, and 4,6-DMDBT) in model oil. The effects of different loadings, reaction temperatures, catalyst dosage, and different desulfurization systems on the desulfurization were systematically investigated. At the same time, the recycling performance of the catalyst and the catalytic oxidation mechanism are discussed.

2. Experimental section

2.1 Materials and characterization methods

All materials and reagents used in this work were obtained from commercial suppliers and used without further purification. Following is the list of materials and reagents. Cobaltous nitrate hexahydrate ($Co(NO_3)_2\cdot 6H_2O$, 98.5%, Sinopharm Chemical Reagent Co., Ltd), 2-methylimidazole (98%, Aladdin), benzothiophene (BT, 98%, Macklin), dibenzothiophene (DBT, 99%, Macklin), 4,6-dimethyldibenzothiophene (4,6-DMDBT, 97%, Macklin), polyethylene glycol 200 (PEG-200, Sinopharm Chemical Reagent Co., Ltd), methanol, (MeOH, 99.5%, Sinopharm Chemical Reagent Co., Ltd), ethanol (MtOH, 99.7%, Sinopharm Chemical Reagent Co., Ltd), *N*-octane (98%, Sinopharm Chemical Reagent Co., Ltd), hydrogen peroxide (H_2O_2, 30 wt%, Sinopharm Chemical Reagent Co., Ltd), tungstosilicic acid hydrate ($H_4SiW_{12}O_{40}\cdot nH_2O$, AR, Macklin), tetrabutylammonium chloride (Bu_4NCl, TBAC, 98%, Accela).

FT-IR spectra of the catalysts (KBr pellets) were recorded using a Nicolet 6700 (Thermo Fisher, USA) FT-IR instrument in the wave number range of 4000–400 cm^{-1} for the determination of the functional groups. X-ray diffraction (XRD) was performed on an Empyrean X-ray diffractometer (Bruker D8 Advance, Germany) with a high-intensity Cu Kα source. Inductively coupled plasma optical emission spectroscopy (ICP-OES) to quantify W concentrations in various samples was performed using an Agilent 5110 (Agilent, USA) instrument. The Brunauer–Emmett–Teller (BET) surface area of the catalyst was obtained from the nitrogen adsorption–desorption isotherms. The nitrogen adsorption–desorption isotherms were collected on BELSORP Max II (MicrotracBEL, Japan). The samples were degassed at 423 K for 4 h, and then the specific surface area and pore structure were determined at 77 K. Scanning electron microscopy (SEM) and electron dispersive X-ray spectroscopy (EDS) analysis were performed on a Gemini SEM 360 (ZEISS, Germany) microscope and an Oxford Xplore 30 spectrometer connected to the microscope, respectively.

2.2 Material preparation

2.2.1 Preparation of silicotungstate ($(TBA)_4SiW_{12}O_{40}$). Silicotungstate was synthesized in one step according to the previous study.[41] 0.5 mmol (1.439 g) $H_4SiW_{12}O_{40}\cdot nH_2O$ was dissolved in 15 mL deionized water, and then the solution of 2.0 mmol TBAC (0.556 g) in 15 mL deionized water was dropwise added to the above solution under magnetic stirring. After stirring for 2 hours, the white emulsion was centrifuged and washed with deionized water and ethanol and dried overnight at 60 °C to obtain a white powder.

2.2.2 Preparation of DES. At a molar ratio of 1 : 2, the corresponding mass of TBAC and the corresponding volume of PEG-200 were placed in a round bottom flask and magnetically stirred for 100 min at 80 °C to produce a colorless transparent liquid DES.

2.2.3 Preparation of ZIF-67. ZIF-67 was prepared by an adaptation of the previously reported experimental procedure.[40,42] Typically, solutions of $Co(NO_3)_2\cdot 6H_2O$ (2.5 mmol) in MeOH (25 mL) were stirred magnetically for 30 min. Afterward, solutions of 2-methylimidazole (20 mmol) in MeOH (25 mL) were slowly added to the above solutions. The mixtures were stirred for 24 h, at room temperature and ambient pressure. Finally, the obtained purple solids were isolated by centrifugation, washed with MeOH and EtOH, and dried under vacuum at 60 °C for 12 h.

2.2.4 Preparation of composite materials. According to previous reports, the composite material was prepared by an adaptation of the previously reported experimental procedure.[2,43] A certain amount of $(TBA)_4SiW_{12}O_{40}$ (90 mg, 180 mg, 270 mg, or 360 mg) was ultrasonically dispersed in MeOH (25 mL) solution containing $Co(NO_3)_2\cdot 6H_2O$ (2.5 mmol). 2-Methylimidazole (20 mmol) was dissolved in MeOH (25 mL) and slowly added to the above solution. The mixture was stirred at room temperature for 24 h. Purple solids were obtained by centrifugation, washed with methanol and ethanol, and dried at 60 °C for 12 hours. Finally, a series of composites (x%-SiW_{12}@ZIF-67) were obtained.

2.3 Oxidative desulfurization studies

The principle of oxidative desulfurization (ODS) technology involves the use of oxidants to oxidize aromatic sulfides into more polar sulfoxides or sulfones, and then separate the

product from the fuel by adsorption, extraction, or other methods.[19,44,45] Commonly used oxidants are air, oxygen, hydrogen peroxide, and oxone. Among them, hydrogen peroxide has the advantages of high efficiency, low cost, and no pollution to the environment, and is widely used in the study of oxidative desulfurization. In addition, hydrogen peroxide can form a catalytic oxidative desulfurization system with oxometallate, organic acids, or heteropolyacids, and the generated active species (transition active components, $^{\cdot}OH$, $^{\cdot}O_2^-$ — *etc.*) can more efficiently remove sulfides.[46–48] Presently, oxidative desulfurization, as a non-hydrodesulfurization technology, is extensively utilized in desulfurization applications due to its mild operational conditions, straightforward process, and high desulfurization efficiency, particularly its effective removal of thiophene sulfides.

The oxidation desulfurization procedure followed in this work is as follows. BT, DBT, 4,6-DMDBT were dissolved in *n*-octane to prepare model oil with sulfur contents of 250 ppm, 500 ppm and 250 ppm, respectively. The reaction was performed in a 50 mL borosilicate closed container with a magnetic stirrer in the air and immersed in a constant temperature water bath at 60 °C. Oxidative catalytic desulfurization experiments were performed in a biphasic system composed of the model oil and the extraction solvent. In a typical experiment, a certain amount of the catalyst material was added to 2 mL of EDS and 5 mL of model oil, and this mixture was stirred for 15 min at 60 °C. Then, the addition of 64 μL of 30% H_2O_2 initiates the catalytic oxidation process. At the end of each reaction, the upper oil phase was taken for GC analysis (GC-2019A). At the same time, the catalyst was recycled after simple treatment and applied to ECODS (extraction, and catalytic oxidative desulfurization system) again under the same reaction conditions. The desulfurization efficiency could be calculated by the following formula: $S\% = (S_0 - S_t)/S_0 \times 100$. Where S_0 is the initial sulfur content in the model oil, and S_t is the sulfur content in the model oil at time t.

3. Results and discussion

3.1 Characterization results and analysis

The FT-IR spectrum, as shown in Fig. 1, was collected to detect the structure of the synthesized catalyst and the functional groups present. In the FT-IR spectrum of ZIF-67, the strong peak at 426 cm^{-1} is attributed to the stretching vibration of the Co–N group formed by the coordination between the Co cluster and the ligand.[42] Several strong peaks at 990–1575 cm^{-1} are attributed to the imidazole ring, which is a typical vibrational bond of ZIF-67. For $(TBA)_4SiW_{12}O_{40}$, polyoxometalate anions produce some characteristic peaks in the range of 800–1100 cm^{-1}. Specifically, the peak at 1012 cm^{-1} is attributed to the Si–O bond, and the peak at 960 cm^{-1} is the stretching vibration of the W=O bond.[27] It is worth noting that compared with pure ZIF-67, all composites *x*%-SiW_{12}@ZIF-67 showed two characteristic peaks belonging to polyoxometalate anions (W–O–W) at 801 and 883 cm^{-1}, and the intensity of the peaks increased with the increase of the $(TBA)_4SiW_{12}O_{40}$ content.[31]

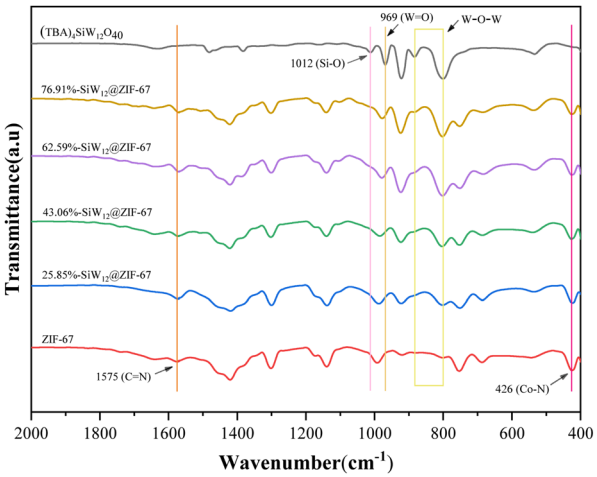

Fig. 1 FT-IR spectra of ZIF-67, $(TBA)_4SiW_{12}O_{40}$ and *x*%-SiW_{12}@ZIF-67.

The XRD patterns of $(TBA)_4SiW_{12}O_{40}$, ZIF-67, and composite *x*%-SiW_{12}@ZIF-67 in the range of 5–50° are shown in Fig. 2. In the XRD pattern of $(TBA)_4SiW_{12}O_{40}$, the characteristic peaks of $(TBA)_4SiW_{12}O_{40}$ with a Keggin structure are shown between 5-10°.[41] The diffraction peaks of ZIF-67 at 2θ of 7.4°, 10.4°, 12.8°, 14.8°, 16.5°, 18.1°, 22.2°, 24.5°, 26.7°, and 29.7° are associated with the (011), (002), (112), (022), (013), (222), (114), (233), (134) and (044) crystal planes, respectively, which is consistent with the diffraction patterns of these crystal structures reported previously, revealing the expected characteristic peaks with correct relative intensity.[49] Compared with the XRD patterns of pure ZIF-67, the results show that there is no significant change in the crystal structure after encapsulation of the active component $(TBA)_4SiW_{12}O_{40}$, indicating that the introduction of $(TBA)_4SiW_{12}O_{40}$ does not affect the structure of the carrier. Notably, the peaks of the samples significantly broadened with the increase of the $(TBA)_4SiW_{12}O_{40}$ content, indicating that the crystallinity of the composites decreased with the increase in the amount of the introduced material. This suggests that a high concentration of $(TBA)_4SiW_{12}O_{40}$ interacts with Co

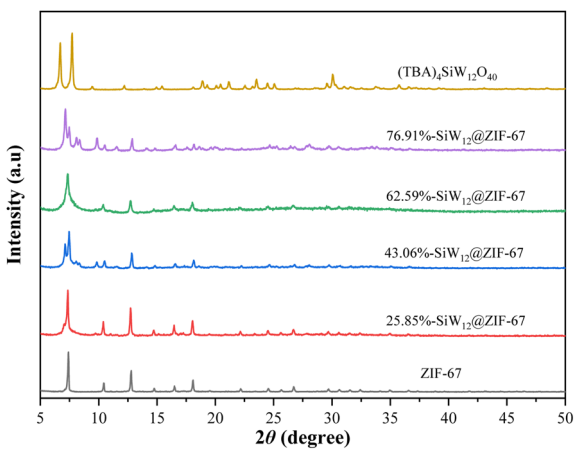

Fig. 2 XRD spectra of ZIF-67, $(TBA)_4SiW_{12}O_{40}$ and *x*%-SiW_{12}@ZIF-67.

clusters and thus inhibits the coordination of 2-methylimidazole ligand to Co clusters.

The morphology of $(TBA)_4SiW_{12}O_{40}$, ZIF-67, and ZIF-67-loaded $(TBA)_4SiW_{12}O_{40}$ was observed by SEM (Fig. 3). The surface morphology of $(TBA)_4SiW_{12}O_{40}$ showed a flocculent structure, which was attributed to the fact that all the silicotungstic acid anions were covered by a large number of carbon chains with lipophilic properties. The surface morphology of

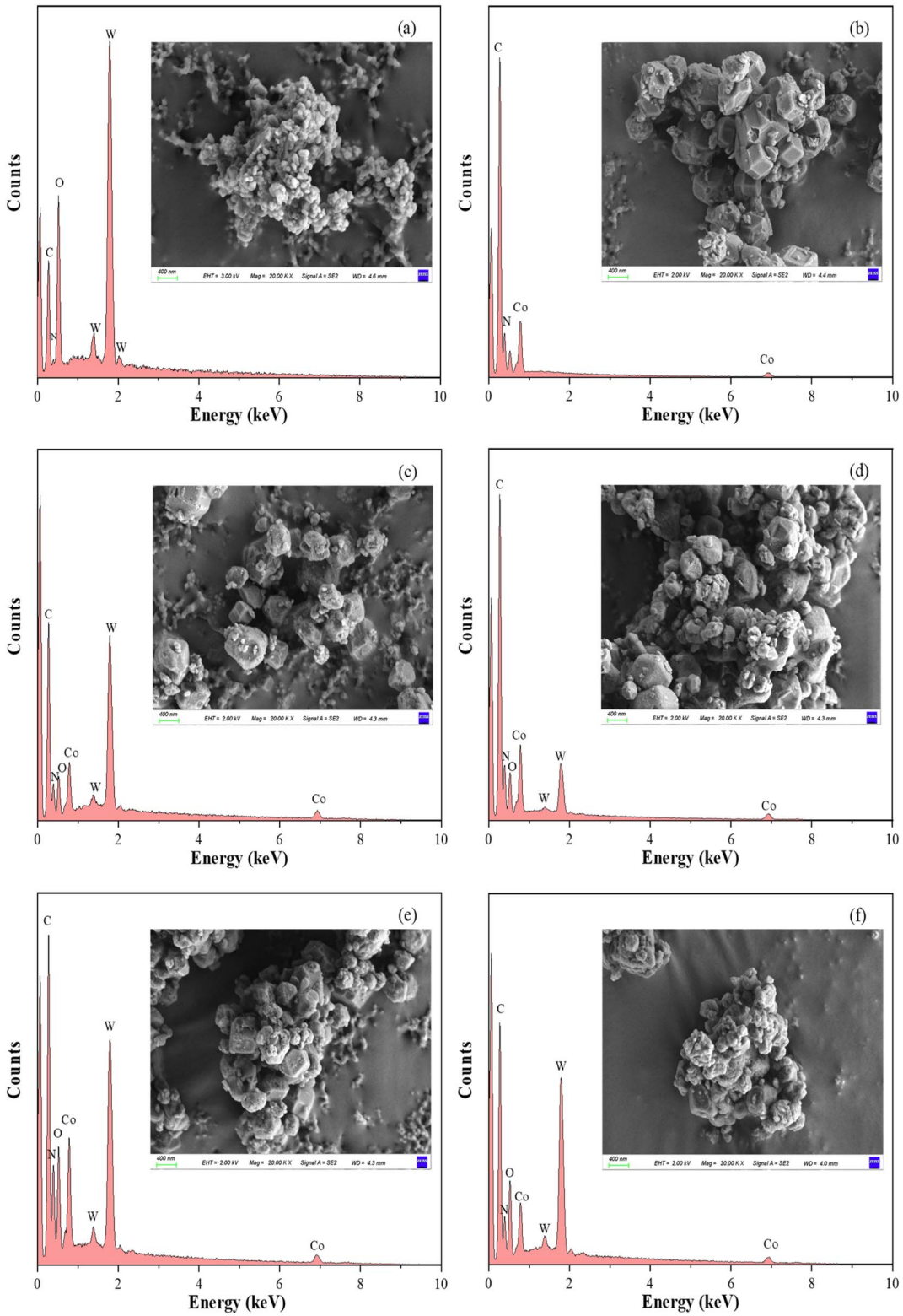

Fig. 3 SEM images and corresponding EDS spectra recorded for $(TBA)_4SiW_{12}O_{40}$ (a), ZIF-67 (b), 25.85%-SiW_{12}@ZIF-67 (c), 43.06%-SiW_{12}@ZIF-67 (d), 62.59%-SiW_{12}@ZIF-67 (e) and 76.91%-SiW_{12}@ZIF-67 (f).

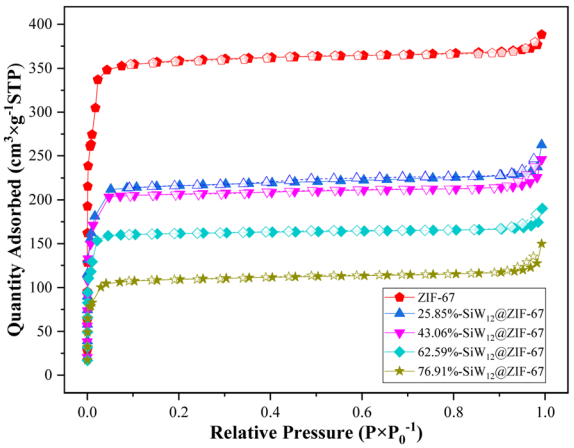

Fig. 4 Nitrogen adsorption–desorption isotherms of ZIF-67 and *x*%-SiW_{12}@ZIF-67.

ZIF-67 depicted uniform rhombic dodecahedrons with smooth surfaces and ideal crystalline features, and the materials were apparently not aggregated. For *x*%-SiW_{12}@ZIF-67, with an increase in loading, the material morphology gradually changed from hexagonal to irregular, and the particles appeared agglomerated, which further verified the XRD results that the crystallinity of ZIF-67 decreased with the increase in the concentration of $(TBA)_4SiW_{12}O_{40}$ during the synthesis process. The successful loading and loading difference of $(TBA)_4SiW_{12}O_{40}$ were further verified through EDS. EDS results confirmed the presence of W, thereby verifying the successful loading of the active component. SEM images revealed a gradual increase in the W/Co peak height ratio, which verified the changing trend of $(TBA)_4SiW_{12}O_{40}$ loading and the analysis of the FT-IR spectrum.

Fig. 4 illustrates that the adsorption and desorption isotherms of ZIF-67 and *x*%-SiW_{12}@ZIF-67 exhibit similarities to type I, which was indicative of the structure of micropores. The specific surface area, pore size, and pore volume were determined through the Brunauer–Emmett–Teller (BET) method (Table 1). As illustrated in Table 1, the specific surface area and pore volume of the composites *x*%-SiW_{12}@ZIF-67 prepared *via* the *in situ* method exhibited a gradual decline with an increase in $(TBA)_4SiW_{12}O_{40}$ loading. This phenomenon was attributed to the occupation of the respective porous channels or cavities by $(TBA)_4SiW_{12}O_{40}$, which verified the analysis of SEM.

Table 1 BET surface area, pore diameter and pore volume of various samples

Samples	Surface area ($m^2\ g^{-1}$)	Pore diameter (nm)	Pore volume ($cm^3\ g^{-1}$)
ZIF-67	1460	1.6314	0.5955
25.85%-SiW_{12}@ZIF-67	850.34	1.8622	0.3959
43.06%-SiW_{12}@ZIF-67	820.44	1.8183	0.3729
62.59%-SiW_{12}@ZIF-67	665.36	1.7079	0.2841
76.91%-SiW_{12}@ZIF-67	425.90	2.0972	0.2233

3.2 Desulfurization studies

3.2.1 Removal effect of different desulfurization systems on DBT in the model oil. In order to investigate the influence of different desulfurization systems on the desulfurization effect, a series of catalysts synthesized were tested for their desulfurization performance under typical experimental conditions, and the results are shown in Table 2. After adding $(TBA)_4SiW_{12}O_{40}$ to the desulfurization system for the reaction, the desulfurization rate was improved to some extent. In contrast, ZIF-67 did not show significant catalytic activity, and the desulfurization rate was only 75.50%. An appropriate increase of $(TBA)_4SiW_{12}O_{40}$ loading can effectively improve the desulfurization efficiency, and the highest removal rate of DBT reached 97.59%. When the $(TBA)_4SiW_{12}O_{40}$ loading was further increased, the desulfurization rate was decreased, which was attributed to the agglomeration of the catalyst, reducing the catalytic activity. Therefore 43.06%-SiW_{12}@ZIF-67 was chosen for the following experiments to optimize the experimental conditions.

3.2.2 Effects of different reaction conditions on desulfurization efficiency. The data on the effect of reaction temperature on the desulfurization efficiency is shown in Fig. 5a. When the reaction temperature was 40 °C, the desulfurization rate was only 73.13%, so the lower temperature is not conducive to the extraction and oxidation reaction. With the increase in the reaction temperature, the probability of intermolecular collision increases, and the desulfurization rate gradually increases. When the temperature rises to 60 °C, the desulfurization rate reaches 97.59%. When the temperature is 70 °C, the desulfurization rate decreases slightly, which may be the gradual decomposition of H_2O_2 at higher temperatures, and the utilization rate of H_2O_2 decreases.[50] Appropriately increasing the reaction temperature is conducive to the desulfurization reaction, so 60 °C was selected as the most suitable reaction temperature.

The effect of the oxidant dosage on the removal of DBT in the model oil is shown in Fig. 5b. The desulfurization reaction was carried out without adding H_2O_2 to the system, and the desulfurization efficiency was only 65.72%, which was the result of the combined effect of the catalyst and the extractant. When the O/S molar ratio was increased from 0 to 6, the conversion of

Table 2 Removal of DBT from model oil using different desulfurization systems[a]

Entry	Catalyst	Sulfur removal (%)
1	No	72.80
2	ZIF-67	75.50
3	$(TBA)_4SiW_{12}O_{40}$	84.95
4	25.85%-SiW_{12}@ZIF-67	88.41
5	43.06%-SiW_{12}@ZIF-67	97.59
6	62.59%-SiW_{12}@ZIF-67	95.23
7	76.91%-SiW_{12}@ZIF-67	91.14

[a] Reaction conditions: $m_{(catalyst)} = 20$ mg; $T = 60$ °C; $t = 75$ min; O/S = 8; $V_{(oil)} = 5$ mL; $V_{(DES)} = 2$ mL.

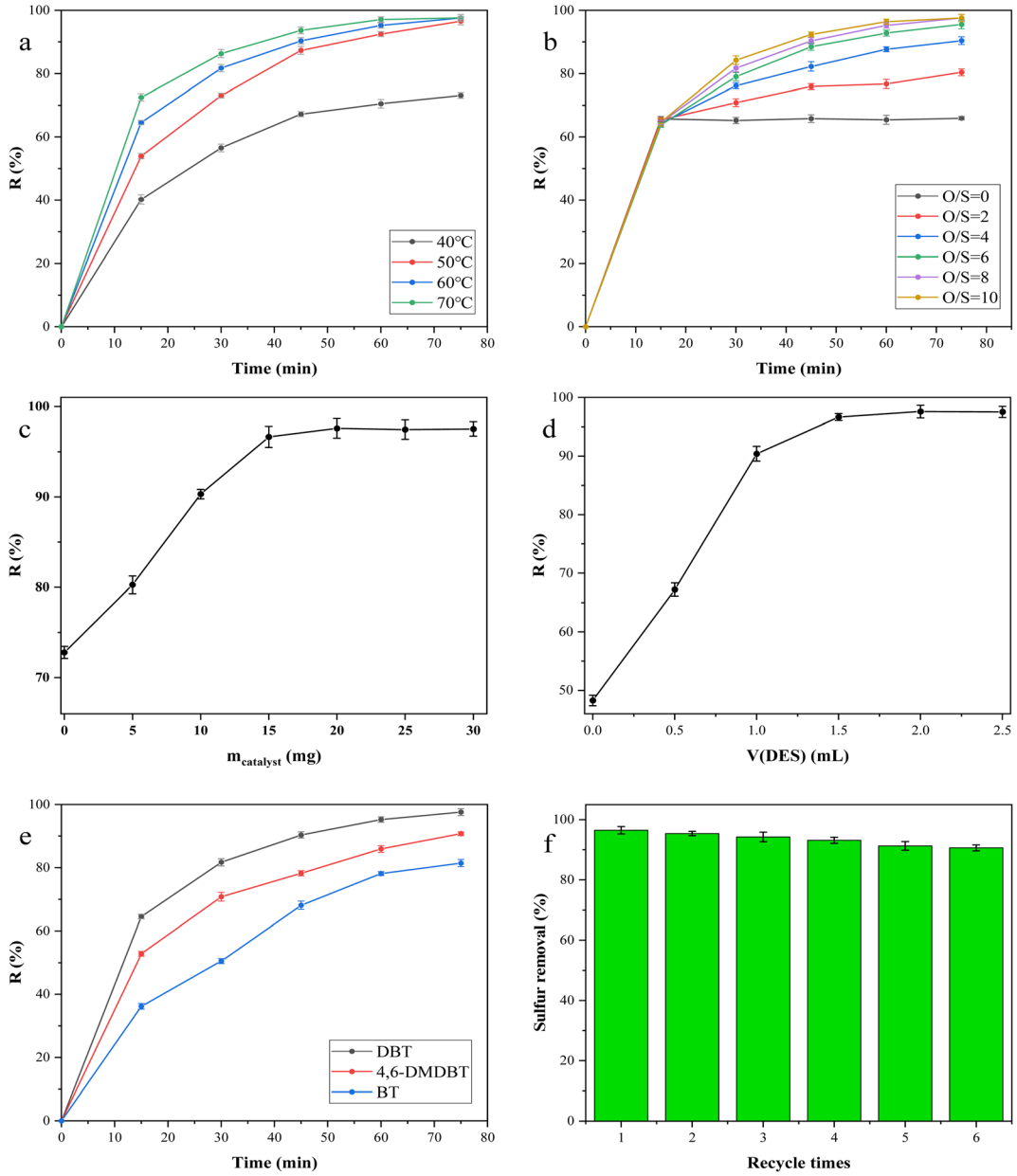

Fig. 5 Effect of different conditions on desulfurization efficiency: reaction temperature (a), O/S molar ratio (b), catalyst dosage (c), extractant dosage (d), different sulfides (e) and cycle times of the catalyst (f).

DBT was significantly increased. When n(O)/n(S) was further increased to 8, the removal of DBT could reach 97.59%. According to the stoichiometric reaction, the oxidation of 1 mol DBT to the corresponding sulfone requires 2 mol H_2O_2.[51] Theoretically, an excess of H_2O_2 is beneficial for the complete oxidation of DBT to sulfone. However, in practice, the excess H_2O_2 will have a certain dilution effect on the catalyst, thus affecting the desulfurization efficiency per unit time. Therefore, considering the overall desulfurization efficiency and cost, n(O)/n(S) = 8 was chosen as the most suitable one.

Fig. 5c illustrates the impact of the catalyst dosage on desulfurization efficiency. Without the catalyst addition to the reaction system, the desulfurization rate is 72.80%, reflecting the collective influence of the oxidant and extractant. The removal efficiency of DBT demonstrated a positive correlation with the dosage of the catalyst. Nevertheless, when the catalyst dosage exceeded 20 mg, the desulfurization effect remained relatively constant. Accordingly, the optimal catalyst dosage was identified as 20 mg.

The effect of extractant dosage on the removal of DBT in model oil is shown in Fig. 5d. In the absence of the extractant, the removal rate of DBT was only 48.27%, which was the result of the combined action of the catalyst and the oxidant. With the increase in the dosage of the extractant, the desulfurization rate is obviously improved. Because the environment similar to a microemulsion is formed after the extractant is added to the

Table 3 Comparison of desulfurization efficiency with references

Catalyst	Oxidant	Extractant	M_c/V_O[a] (g L^{-1})	O/S	E/V[b]	T (°C)	t (min)	Catalyst recovery	R (%)	Ref.
$H_4SiW_{12}O_{40}$	H_2O_2	—	20	8	—	50	90	—	23.58	41
$(HTA)_4SiWO_{40}$	H_2O_2	—	20	10	—	50	75	4	98.4	41
$(TBA)_4SiWO_{40}$	H_2O_2	DES	4	8	2 : 5	60	75	—	85.0	This work
40-HPMo@ZIF-67	TBHP[c]	MeCN	10	8	1 : 5	70	180	5	96.0	53
AC/ZIF-67	TBHP[c]	MeCN	5	20	1 : 2	60	60	5	98.1	54
AC/ZIF-67	H_2O_2	MeCN	5	20	1 : 2	60	60	—	96.0	54
27.5%-PW_4@ZIF-8	H_2O_2	[BMIM]PF_6	13.3	5	1 : 1	70	60	10	98.9	43
43.06%-SiW_{12}@ZIF-67	H_2O_2	DES	4	8	2 : 5	60	75	6	97.6	This work

[a] $M_{catalyst}/V_{oil}$ chem. [b] $V_{Extractant}/V_{oil}$ [c] t-Butylhydro peroxide.

reaction system. This environment can effectively increase the contact among catalysts, oxidants, and sulfides, thereby improving the desulfurization efficiency. When the dosage of the extractant is more than 2.0 mL, the trend of increase in desulfurization efficiency gradually eases. The reason may be that excessive DES dilutes H_2O_2.[52]

Table 3 compares the DBT removal efficiency of the catalyst 43.06%-SiW_{12}@ZIF-67 with other POM and ZIF-based catalysts described in the literature. It can be seen that the desulfurization efficiency of 43.06%-SiW_{12}@ZIF-67 synthesized in this work is better than that of the 40-HPMo@ZIF-67. At the same time, the reaction time of the desulfurization process is shorter, the dosage of the catalyst is less, and the oxidant is more environmentally friendly. Compared with that from ref. 41, the catalyst prepared in this work has better cycle performance. In addition, DES has the advantages of low consumption, high stability, and non-toxicity compared to the extractants used in ref. 43 and 54. Therefore, the desulfurization system studied in this work can effectively achieve deep desulfurization.

In addition to the typical DBT, BT and 4,6-DMDBT were also removed under the optimal reaction conditions, as shown in Fig. 5e. The removal rates of DBT, 4,6-DMDBT, and BT reached 97.59%, 90.78%, and 81.45%, respectively. According to the literature, the electron densities on the sulfur atoms of 4,6-DMDBT, DBT, and BT are 5.760, 5.758, and 5.739, respectively.[55–57] Although the electron cloud density of 4,6-DMDBT is higher than that of DBT, its desulfurization rate is lower than that of DBT. This may be due to the presence of two methyl groups, which increases the steric hindrance and makes the removal efficiency of 4,6-DMDBT slightly worse.

3.3 Catalyst circulation and stability

The cycle performance of the catalyst was tested under the selected optimal reaction conditions. After each desulfurization reaction, the upper oil phase was taken for sulfur content detection and analysis, and the extraction phase was separated from the bottom of the liquid separation funnel by the liquid separation funnel. The solvent in the system was separated from the catalyst by the centrifugation–precipitation method, and the catalyst was washed with ethanol and dried at 60 °C to obtain a reusable catalyst. The number of repeated uses of the catalyst and its effect on the desulfurization efficiency are shown in Fig. 5f. After 6 consecutive cycles, the desulfurization rate of DBT still reached 90.62%. Fig. 6a is the FT-IR spectrum of the recycled catalyst and the fresh catalyst. The strong peak at 426 cm^{-1} is attributed to the stretching vibration of the Co–N group. Two characteristic peaks at 803 and 887 cm^{-1} belong to the W–O–W bond. The peak at 985 cm^{-1} is the stretching vibration of the W=O bond and the peak at 1571 cm^{-1} is attributed to the stretching vibration of C=N bonds. The peaks at 2859 cm^{-1}, 2932 cm^{-1} and 3133 cm^{-1} are associated with the C–H stretching vibrations of the aliphatic chain and the aromatic ring. The presence of bonded water in the samples may be the cause of the peaks observed in the range of 3250–3750 cm^{-1}.[58,59] After recycling, the structure of the catalyst was not significantly damaged. Notably, several peaks of the recycled catalyst observed at 1141 cm^{-1}, 1176 cm^{-1} and 1278 cm^{-1} are attributed to the bending vibrations of the S=O bond in oxidation products.[60,61] It shows that there are oxidation products accumulated in the recycled catalyst. At the same time, the SEM images (Fig. 6c and d) of the recycled catalyst also verify this view. In addition, the continuous accumulation of the oxidation products may also be the main reason for the decrease in the desulfurization rate of the recycled catalyst. In summary, the catalyst has good catalytic activity and cycling stability.

3.4 Analysis of oxidation products and desulfurization mechanism

Upon addition of water to the extraction phase from which the catalyst was separated, a white solid precipitates as the sulfide has a different solubility in the two liquids. The oxidation products of DBT were obtained by filtration and drying. The FT-IR spectra of the product and DBT are shown in Fig. 6b and the reaction products have similar functional groups to DBT, with the peaks at 1288 cm^{-1}, 1166 cm^{-1}, and 1046 cm^{-1} attributed to the S=O bond in $DBTO_2$. Based on the above conclusions and related literature reports, the reaction mechanism of ECODS was assumed, as shown in Fig. 7.[28,33,62,63] It is assumed that in the desulfurization system, DBT is first extracted into the extraction phase by the extractant. At the same time, the catalyst

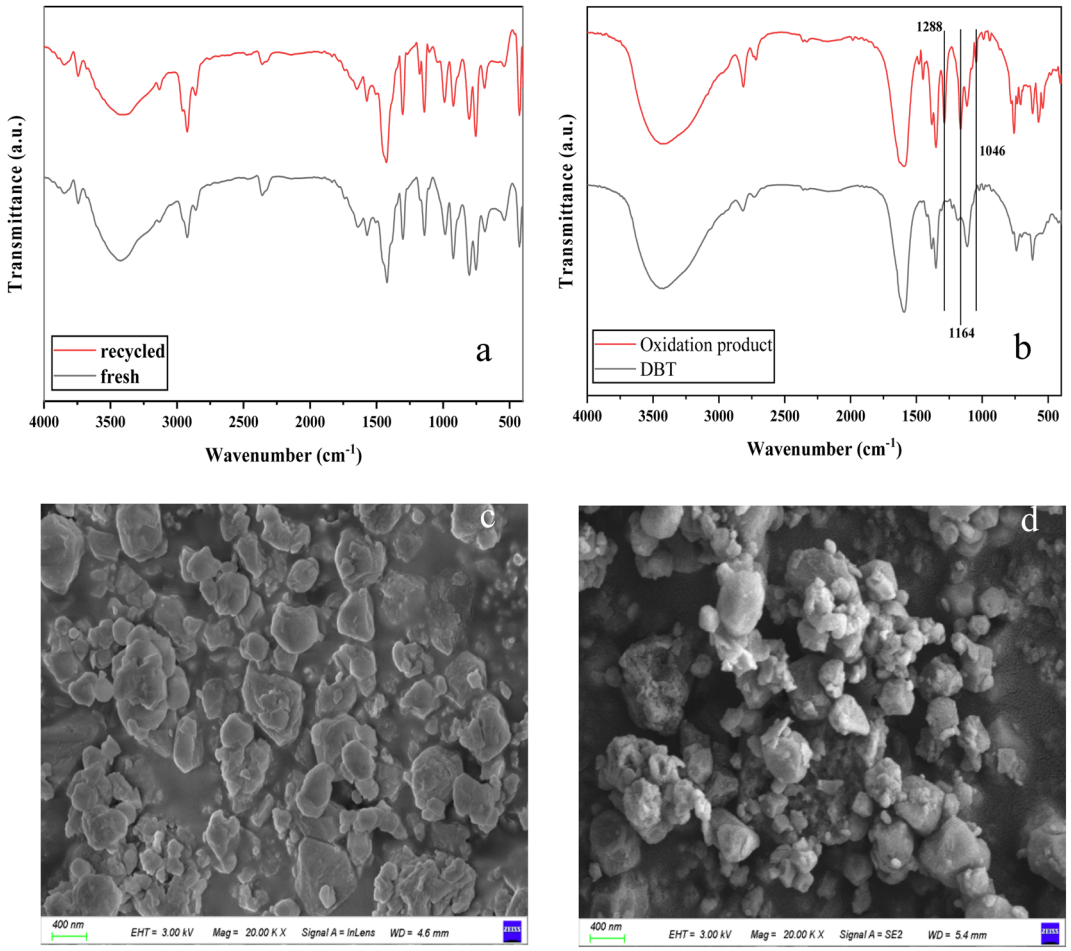

Fig. 6 FT-IR spectra of the fresh and recycled catalyst (a), DBT and oxidation product (b) and SEM images of the recycled catalyst (c and d).

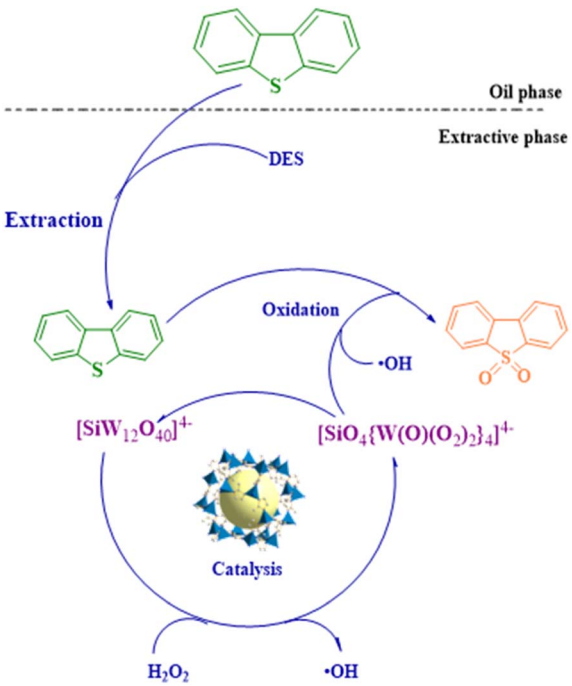

Fig. 7 Proposed mechanism for the oxidation of DBT in ECODS.

with a large specific surface dispersed in the extraction phase area adsorbs sulfide. Besides, the quaternary ammonium silicotungstate of the catalyst has good amphiphilicity, which can make the extraction phase, catalyst, and model oil more fully mixed. In the following catalytic oxidation process, the silicotungstate anion $[SiW_{12}O_{40}]^{4-}$ in the composite catalyst is oxidized by H_2O_2 to generate peroxide $[SiO_4\{W(O)(O_2)_2\}_4]^{4-}$, while H_2O_2 is activated by the catalyst to form catalytically active oxygen species (possibly $^{\bullet}OH$). Then, through the redox reaction among DBT, $[SiO_4\{W(O)(O_2)_2\}_4]^{4-}$, and $^{\bullet}OH$, DBT was selectively oxidized to $DBTO_2$, and $[SiO_4\{W(O)(O_2)_2\}_4]^{4-}$ was reduced to the original $[SiW_{12}O_{40}]^{4-}$. As the reaction proceeds, DBT is continuously oxidized and extracted, and the content of DBT in the oil phase continues to decrease, while the oxidation product $DBTO_2$ continues to accumulate in the extraction phase until the end of the reaction.

4. Conclusions

In summary, composites (x%-SiW_{12}@ZIF-67, x = 25.85, 43.06, 62.59, and 76.91) were prepared by *in situ* synthesis and used as heterogenous catalysts for ECODS. The catalysts were characterized by FT-IR, XRD, BET, and SEM, and it was verified that the

active component $(TBA)_4SiW_{12}O_{40}$ was successfully loaded in the pores of ZIF-67. The carrier ZIF-67 did not show significant activity for DBT removal, and the composite x%-SiW_{12}@ZIF-67 showed significant catalytic activity for sulfide removal, indicating that the $(TBA)_4SiW_{12}O_{40}$ in the catalyst is the key factor for the high activity of the catalyst. The increase in the content of the active component $(TBA)_4SiW_{12}O_{40}$ in the catalyst improved the catalytic activity to a certain extent. However, when the content of the active component is too high, it may lead to the clogging of the ZIF-67 chamber and decrease the reactant diffusion rate, which leads to the decrease of the catalytic activity. Among the catalysts, 43.06%-SiW_{12}@ZIF-67 showed good catalytic activity for DBT, 4,6-DMDBT, and BT, with desulfurization rates of 97.59%, 90.78% and 81.45%, respectively, at $m_{(catalyst)} = 20$ mg, $T = 60$ °C, $t = 75$ min, O/S = 8, $V_{(oil)} = 5$ mL, and $V_{(DES)} = 2$ mL. The desulfurization efficiency of different sulfides was affected by the electron density and the spatial site resistance of sulfur, and the window size of ZIF-67. In addition, the catalyst has good reusability and structural stability, and the removal rate of DBT can still reach more than 90% after 6 consecutive cycles.

Data availability

The data are available from the corresponding author upon reasonable request.

Conflicts of interest

The authors declare no conflict of interest.

Acknowledgements

This study has been partially financed by the Hubei Natural Science Foundation Project (2013CKB032) and the Doctoral Program of Hubei University of Technology (200701).

References

1 F. Johnsson, J. Kjärstad and J. Rootzén, The threat to climate change mitigation posed by the abundance of fossil fuels, *Clim. Pol.*, 2019, **19**(2), 258–274.
2 Y. Gao, *et al.*, Peroxomolybdate@MOFs as effective catalysts for oxidative desulfurization of fuels: correlation between MOF structure and catalytic activity, *Catal. Sci. Technol.*, 2023, **13**(16), 4785–4801.
3 X. Chen, J. Zhang and H. Wei, Physiological responses of earthworm under acid rain stress, *Int. J. Environ. Res. Publ. Health*, 2020, **17**(19), 7246.
4 X. Liu, *et al.*, Oxidative desulfurization of fuel oil catalyzed by a carbon nitride supported phosphotungstic acid based dicationic ionic liquid, *React. Chem. Eng.*, 2022, **7**(6), 1380–1390.
5 S. Rajasuriyan, *et al.*, Oxidative extractive desulfurization system for fuel oil using acidic eutectic-based ionic liquid, *Processes*, 2021, **9**(6), 1050.
6 Y. Gao, *et al.*, Peroxo-polyoxometalate encapsulated within zirconium-based metal organic frameworks for extractive and oxidative desulfurization of fuels, *Chem. Eng. Sci.*, 2024, **284**, 119524.
7 M. F. Majid, *et al.*, Futuristic advance and perspective of deep eutectic solvent for extractive desulfurization of fuel oil: A review, *J. Mol. Liq.*, 2020, **306**, 112870.
8 F. Boshagh, *et al.*, Key factors affecting the development of oxidative desulfurization of liquid fuels: a critical review, *Energy Fuels*, 2021, **36**(1), 98–132.
9 S. Majodina, Z. R. Tshentu and A. S. Ogunlaja, Effect of adding chelating ligands on the catalytic performance of Rh-promoted MoS_2 in the hydrodesulfurization of dibenzothiophene, *Catalysts*, 2021, **11**(11), 1398.
10 Z. Bai, *et al.*, Symbiosis of 1T and 2H phases in the basal plane of defective MoS_2 nanoflowers for efficient hydrodesulfurization, *Fuel*, 2022, **322**, 124252.
11 H. A. Al-Jamimi, G. M. BinMakhashen and T. A. Saleh, Multiobjectives optimization in petroleum refinery catalytic desulfurization using Machine learning approach, *Fuel*, 2022, **322**, 124088.
12 J. C. García-Martínez, *et al.*, Hydrodesulfurization of 4,6–Dimethyldibenzothiophene on NiMoP/γ–Al_2O_3 catalyst under reactive distillation conditions in a micro trickle bed reactor: solvent and temperature effect, *Int. J. Chem. React. Eng. C*, 2023, **21**(4), 413–429.
13 A. Haruna, Z. M. A. Merican and G. M. Suleiman, Recent advances in catalytic oxidative desulfurization of fuel oil–A review, *J. Ind. Eng. Chem.*, 2022, **112**, 20–36.
14 S. A. Ganiyu and A. L. Saheed, Review of adsorptive desulfurization process: Overview of the non-carbonaceous materials, mechanism and synthesis strategies, *Fuel*, 2021, **294**, 120273.
15 K. Zhou, *et al.*, Synthesis of mesoporous ZnO/TiO_2–SiO_2 composite material and its application in photocatalytic adsorption desulfurization without the addition of an extra oxidant, *Dalton Trans.*, 2020, **49**(5), 1600–1612.
16 M. Ahmadian and M. Anbia, Oxidative desulfurization of liquid fuels using polyoxometalate-based catalysts: a review, *Energy Fuels*, 2021, **35**(13), 10347–10373.
17 C. Dai, *et al.*, Ionic liquids in selective oxidation: catalysts and solvents, *Chem. Rev.*, 2017, **117**(10), 6929–6983.
18 A. Haruna, Z. M. A. Merican and G. M. Suleiman, Recent advances in catalytic oxidative desulfurization of fuel oil–A review, *J. Ind. Eng. Chem.*, 2022, **112**, 20–36.
19 A. Guntida, *et al.*, Catalytic oxidative desulfurization of liquid fuel: Impact of oxidants, extracting agents, and heterogeneous catalysts with prospects for biodiesel upgrading-A mini review, *Biomass Bioenergy*, 2024, **188**, 107341.
20 Y. Guo, *et al.*, Optimization study on deep extractive oxidative desulfurization with tetrabutylammonium bromide/polyethylene glycol DES, *RSC Adv.*, 2021, **11**(50), 31727–31737.
21 J. Yin, *et al.*, Deep desulfurization of fuels based on an oxidation/extraction process with acidic deep eutectic solvents, *Green Chem.*, 2015, **17**(9), 4552–4559.

22 F. Lima, *et al.*, Towards a sulfur clean fuel: Deep extraction of thiophene and dibenzothiophene using polyethylene glycol-based deep eutectic solvents, *Fuel*, 2018, **234**, 414–421.
23 W. Liu, *et al.*, One-pot oxidative desulfurization of fuels using dual-acidic deep eutectic solvents, *Fuel*, 2020, **265**, 116967.
24 Y. Hijji, *et al.*, One minute microwave synthesis of $[O_2N\text{-}Ph\text{-}CH_2\text{-}Py{=}N(Me)_2]^+[Cl]^-$ ionic liquid: XRD/HSA-interactions, physicochemical, optical, thermal and A DFT/TD-DFT analysis, *J. Mol. Liq.*, 2021, **339**, 116737.
25 C. Li, *et al.*, Extraction desulfurization process of fuels with ammonium-based deep eutectic solvents, *Green Chem.*, 2013, **15**(10), 2793–2799.
26 W. Jiang, *et al.*, Boric acid-based ternary deep eutectic solvent for extraction and oxidative desulfurization of diesel fuel, *Green Chem.*, 2019, **21**(11), 3074–3080.
27 S. Fernandes, *et al.*, Lindqvist *versus* Keggin-Type Polyoxometalates as Catalysts for Effective Desulfurization of Fuels, *Catalysts*, 2022, **12**(6), 581.
28 Q. Wang, *et al.*, Aerobic Oxidative Desulfurization by Supported Polyoxometalate Ionic Liquid Hybrid Materials *via* Facile Ball Milling, *Molecules*, 2024, **29**(7), 1548.
29 E. Eseva, *et al.*, Deep aerobic oxidative desulfurization of model fuel by Anderson-type polyoxometalate catalysts, *Catal. Commun.*, 2021, **149**, 106256.
30 M. A. Rezvani and N. Khalafi, Deep oxidative desulfurization of real fuel and thiophenic model fuels using polyoxometalate-based catalytic nanohybrid material, *Mater. Today Commun.*, 2020, **22**, 100730.
31 M. Taghizadeh, E. Mehrvarz and A. Taghipour, Polyoxometalate as an effective catalyst for the oxidative desulfurization of liquid fuels: a critical review, *Rev. Chem. Eng.*, 2020, **36**(7), 831–858.
32 Y. Zhu, *et al.*, Phosphotungstic acid supported on mesoporous graphitic carbon nitride as catalyst for oxidative desulfurization of fuel, *Ind. Eng. Chem. Res.*, 2015, **54**(7), 2040–2047.
33 J. Li, *et al.*, Polyoxometalate dicationic ionic liquids as catalyst for extractive coupled catalytic oxidative desulfurization, *Catalysts*, 2021, **11**(3), 356.
34 P. Mialane, *et al.*, Heterogenisation of polyoxometalates and other metal-based complexes in metal–organic frameworks: from synthesis to characterisation and applications in catalysis, *Chem. Soc. Rev.*, 2021, **50**(10), 6152–6220.
35 K. Maru, S. Kalla and R. Jangir, MOF/POM hybrids as catalysts for organic transformations, *Dalton Trans.*, 2022, **51**(32), 11952–11986.
36 A. Haruna, *et al.*, A critical review on recent trends in metal-organic framework-based composites as sustainable catalysts for environmental applications, *J. Environ. Chem. Eng.*, 2024, 113542.
37 S. Mukhopadhyay, *et al.*, A Keggin Polyoxometalate Shows Water Oxidation Activity at Neutral pH: POM@ ZIF-8, an Efficient and Robust Electrocatalyst, *Angew. Chem.*, 2018, **130**(7), 1936–1941.
38 P. Hu, *et al.*, In situ assembled zeolite imidazolate framework nanocrystals hybrid thin film nanocomposite membranes for brackish water desalination, *Sep. Purif. Technol.*, 2022, **293**, 121134.
39 D. Saliba, *et al.*, Crystal growth of ZIF-8, ZIF-67, and their mixed-metal derivatives, *J. Am. Chem. Soc.*, 2018, **140**(5), 1812–1823.
40 A. M. Viana, *et al.*, Effective combination of the metal centers in MOF-based materials toward sustainable oxidation catalysts, *Materials*, 2023, **16**(8), 3133.
41 Y. Guo, X. Liu and B. Hu, Synthesis of modified amphiphilic quaternary ammonium silicotungstate and its application in heterogeneous catalytic oxidative desulfurization, *React. Chem. Eng.*, 2022, **7**(9), 1978–1989.
42 J. Dai, *et al.*, Fabrication of novel ZIF-67 composite microspheres for effective adsorption and solid-phase extraction of dyes from water, *ChemistrySelect*, 2018, **3**(21), 5833–5842.
43 Y. Gao, *et al.*, In situ encapsulation of peroxophosphotungstate in ZIF-8: A highly active, reusable and structurally stable catalyst for desulfurization, *Fuel Process. Technol.*, 2024, **254**, 108033.
44 M. A. Rezvani, S. Hosseini and H. H. Ardeshiri, Highly efficient catalytic oxidative desulfurization of gasoline using $PMnW_{11}$@ PANI@ CS as a new inorganic–organic hybrid nanocatalyst, *Energy Fuels*, 2022, **36**(14), 7722–7732.
45 F.-L. Yu, *et al.*, Oxidative-extractive deep desulfurization of gasoline by functionalized heteropoly acid catalysts, *RSC Adv.*, 2015, **5**(104), 85540–85546.
46 J. Li, *et al.*, Cu (I) anchoring in MOF-808 as a stable catalyst in ultra-deep oxidation desulfurization, *Fuel*, 2023, **341**, 127674.
47 S. Wei, *et al.*, Performances, kinetics and mechanisms of catalytic oxidative desulfurization from oils, *RSC Adv.*, 2016, **6**(105), 103253–103269.
48 Q. Wang, *et al.*, Novel High-Activity Al_2O_3@ Zr X PTA Catalysts and Their Catalytic Oxidative Desulfurization, Mechanism, and Molding, *Ind. Eng. Chem. Res.*, 2023, **62**(6), 2525–2535.
49 K. Zhou, *et al.*, Characterization and properties of Zn/Co zeolitic imidazolate frameworks *vs.* ZIF-8 and ZIF-67, *J. Mater. Chem. A*, 2017, **5**(3), 952–957.
50 H.-Q. Zheng, *et al.*, Zr-based metal–organic frameworks with intrinsic peroxidase-like activity for ultradeep oxidative desulfurization: mechanism of H_2O_2 decomposition, *Inorg. Chem.*, 2019, **58**(10), 6983–6992.
51 Z. Qi, *et al.*, In situ bridging encapsulation of a carboxyl-functionalized phosphotungstic acid ionic liquid in UiO-66: A remarkable catalyst for oxidative desulfurization, *Chem. Eng. Sci.*, 2020, **225**, 115818.
52 J. Xu, *et al.*, Green aerobic oxidative desulfurization of diesel by constructing an Fe-Anderson type polyoxometalate and benzene sulfonic acid-based deep eutectic solvent biomimetic cycle, *Chin. J. Catal.*, 2020, **41**(5), 868–876.
53 M. Jafarinasab and A. Akbari, Co-ZIF-67 encapsulated phosphomolybdic acid as a hybrid catalyst for deep oxidative desulfurization, *J. Environ. Chem. Eng.*, 2021, **9**(6), 106472.

54 M. R. H. Moghaddam and M. Niknam Shahrak, Coupled one-pot oxidative extractive desulfurization of a model fuel catalyzed by nanostructured-ZIF-67/Biomass-derived activated carbon composite, *Inorg. Chem. Commun.*, 2024, **165**, 112489.

55 Z. Yunfeng, *et al.*, Phosphotungstic Acid Supported on Mesoporous Graphitic Carbon Nitride as Catalyst for Oxidative Desulfurization of Fuel, *Ind. Eng. Chem. Res.*, 2015, **54**(7), 2040–2047.

56 S. O. Ribeiro, *et al.*, Oxidative desulfurization strategies using Keggin-type polyoxometalate catalysts: Biphasic *versus* solvent-free systems, *Catal. Today*, 2019, **333**, 226–236.

57 D. Julião, *et al.*, A sustainable peroxophosphomolybdate/H_2O_2 system for the oxidative removal of organosulfur compounds from simulated and real high-sulfur diesels, *Appl. Catal., A*, 2020, **589**, 117154.

58 M. Ammar, S. Jiang and S. Ji, Heteropoly acid encapsulated into zeolite imidazolate framework (ZIF-67) cage as an efficient heterogeneous catalyst for Friedel–Crafts acylation, *J. Solid State Chem.*, 2016, **233**, 303–310.

59 M. Jafarinasab, *et al.*, An efficient Co-based metal–organic framework nanocrystal (Co-ZIF-67) for adsorptive desulfurization of dibenzothiophene: Impact of the preparation approach on structure tuning, *Energy Fuels*, 2020, **34**(10), 12779–12791.

60 L. Hao, *et al.*, L-proline-based deep eutectic solvents (DESs) for deep catalytic oxidative desulfurization (ODS) of diesel, *J. Hazard Mater.*, 2017, **339**, 216–222.

61 S. Xun, *et al.*, Magnetic mesoporous nanospheres supported phosphomolybdate-based ionic liquid for aerobic oxidative desulfurization of fuel, *J. Colloid Interface Sci.*, 2019, **534**, 239–247.

62 A. Akbari, M. Chamack and M. Omidkhah, Reverse microemulsion synthesis of polyoxometalate-based heterogeneous hybrid catalysts for oxidative desulfurization, *J. Mater. Sci.*, 2020, **55**(15), 6513–6524.

63 Y. Guo, X. Liu and B. Hu, Adsorption oxidation desulfurization of model fuel by mesoporous SiO_2 supported deep eutectic solvents TBAB/PEG-200, *New J. Chem.*, 2022, **46**(46), 22143–22150.